Accurate Determination of Photovoltaic Cell and Module Peak Power From Their Current–Voltage Characteristics

Bertrand Paviet-Salomon, Jacques Levrat, Vahid Fakhfouri, Yanik Pelet, Nicolas Rebeaud, Matthieu Despeisse, and Christophe Ballif

***Abstract*—We investigate the extraction of the peak power of photovoltaic (PV) cells and modules from their current–voltage (*I–V*) characteristics. Synthetic *I–V* curves are generated by numerically solving the two-diode equation in steady-state conditions with representative parameters for crystalline silicon-based solar cells. Parasitic effects that may affect the shape of the current–voltage curves are not considered yet. The cases of high- and low-voltage sampling frequencies are addressed. We propose and qualify a novel fit procedure, where the boundaries are defined as two independent power thresholds, and demonstrate a factor 3–4 improvement on the peak power estimation in comparison with other state-of-the-art approaches. We unveil the dependence of the fit accuracy on the devices parameters, especially their fill factor (FF). Interestingly, we show that an equally good fit accuracy is obtained when only five to ten points are placed neighboring the peak power, provided that these points are placed at the appropriate positions. We then broaden our approach to the extraction of the short-circuit current density and the open-circuit voltage from *I–V* curves. We validate our guidelines by extracting the maximum peak power from *(I-V)* curves measured on actual PV devices.**

***Index Terms*—ASTM E948-09 standard, fitting, current-voltage (*I–V*) curve, peak power, polynomials, power rating, silicon, solar cell.**

I. Introduction

THE electrical performances of photovoltaic (PV) cells and modules are assessed by measuring their current–voltage (*I–V*) characteristics under standard test conditions. From the *I–V* curve, the values of the short-circuit current density (J_{sc}), the open-circuit voltage (V_{oc}), and the nominal peak power (P_{max}) at maximum power point (MPP) are usually extracted [1]. The aforementioned parameters are known as the PV cell or module key data and are standardly reported in test certificates or products datasheets.

Among the key data, the accurate determination of P_{max} is of fundamental importance for PV manufacturers, as the PV module selling prices are directly linked to their measured P_{max}. Nowadays, PV manufacturers have typically 5–10% accuracy on P_{max} rating [2], whereas certification laboratories achieve values below 2% [3], [4]. Translating these figures into an economical perspective, every 1% uncertainty in determining P_{max} is worth \$6 million/year for a 1-GW production line, assuming a module price of \$0.6 per watt-peak [5]. With the PV market being rapidly growing, there is, therefore, a strong need in enhancing, more and more, the accuracy and the reliability in determining the solar cells and modules P_{max}.

Several factors are known to affect the accuracy of the PV cell and module rating: temporal and spatial fluctuations of both the spectrum and the irradiance of the light source [6]–[8]; temperature stability of the device under test [6], [8]; contacting issues [6]; reference cells [9], [10]; as well as the acquisition and the postprocessing of the data themselves [1], [3]. For pulsed-light measurements using short flash durations—and consequently, requiring fast sweeping times, typically ≤50 ms—the accurate determination of P_{max} is further complicated by transient effects potentially arising from the capacitive behavior of, for instance, high-performance silicon solar cells [11], [12]. Solutions have, thus, been sought for to circumvent this issue, such as the use of several subsequent short flashes [13], or various correction procedures [14]–[16]. Another way is to use a customized voltage profile, comprising 10–20 voltage plateaus to measure stable current and voltage signals, superimposed to voltage peaks aiming at charging the device capacitance faster, hence obtaining even more stable current values. This elegant approach is known as DragonBack and is investigated in further detail in [17] and [18]. However, it remains to be determined how many data points are actually needed, and where they should be placed along the *I–V* curve, to accurately extract P_{max} from a low-density (LD) *I–V* curve.

Among all the above-mentioned factors affecting the accurate determination of P_{max}, uncertainties linked to the effective irradiance and the actual acquisition of the *I–V* curve play the major role and represent more than 50% of the overall measurement uncertainty [3]. However, for a given *I–V* curve, the algorithms and methods used to extract P_{max} can, in themselves, lead to errors as high as 2–3%, as investigated in [19]–[21]. Table I gives a state of the art of the criteria suggested by various publications and international standards to extract P_{max} from *I–V* curves, as well as the ones we propose in this paper.

To date, a single international standard specifically deals with the extraction of P_{max} from *I–V* curves: the ASTM E948-09 [22].

Manuscript received March 3, 2016; revised May 31, 2016 and June 29, 2016; accepted July 6, 2016.

B. Paviet-Salomon, J. Levrat, M. Despeisse, and C. Ballif are with the PV-Center, Centre Suisse d'Électronique et de Microtechnique, Neuchâtel CH-2002, Switzerland (e-mail: bertrand.paviet-salomon@csem.ch; jacques.levrat@csem.ch; matthieu.despeisse@csem.ch; christophe.ballif@csem.ch).

V. Fakhfouri, Y. Pelet, and N. Rebeaud are with the Meyer Burger Group, Pasan SA, Neuchâtel CH-2000 Switzerland (e-mail: vahid.fakhfouri@meyerburger.com; yanik.pelet@meyerburger.com; nicolas.rebeaud@meyerburger.com).

Color versions of one or more of the figures in this paper are available online at http://ieeexplore.ieee.org.

Digital Object Identifier 10.1109/JPHOTOV.2016.2590940

TABLE I
STATE-OF-THE-ART FIT CRITERIA RECOMMENDED FOR THE EXTRACTION OF THE SOLAR CELLS AND MODULES PEAK POWER FROM THEIR *I–V* CURVES

Ref.	Year	Fit type	Range
			(*J*, *V*) points such that:
ASTM [22]	2009	Fourth-order polynomial	$0.75 \times V_{mpp} < V < 1.15 \times V_{mpp}$ $0.75 \times J_{mpp} < J < 1.15 \times J_{mpp}$
NREL [1]	2011	≥Fourth-order polynomial	(*P*, *V*) points such that $P > 0.8 \times P_{max}$ and $V > 0.8 \times V_{mpp}$
Dirnberger *et al.* [3]	2013	Fifth-order polynomial	No range specified
			(P, V) points such that:
This work	*2016*	*≥Fourth-order polynomial*	$P \geq 0.82 \times P_{max} for\ V < V_{mpp}$ $P \geq 0.94 \times P_{max} for\ V \geq V_{mpp}$

V: voltage; *J*: current density; *P*: power density; V_{mpp} (respectively, J_{mpp}): voltage (respectively, current density) at MPP.

It recommends the use of a fourth-order polynomial fit on a range defined for (*I*, *V*) points. Alternatively, National Renewable Energy Laboratory (NREL) [1] proposes to use a polynomial fit of at least the fourth order, on a range defined for (*P*, *V*) points. Dirnberger and Kraling [3] use a fifth-order polynomial fit, but further details on the fit range and algorithm are undisclosed. Importantly, apart from [3], none of these references provide an estimation of the accuracy that can be achieved following their guidelines. Moreover, they do not explicitly state how these guidelines have to be adjusted as a function of the solar cell and module parameters, or depending on the *I–V* curve characteristics (noise level, sampling frequency, etc.). Finally, they were not proven on *I–V* curves with fewer data points, such as, e.g., the *DragonBack* curves.

In this paper, we aim to determine the fit ranges and methods that yield the highest accuracy for the extraction of P_{max} from *I–V* curves, as well as linking the obtained accuracy to the device electrical parameters. Our approach is based on *I–V* curves generated by numerically solving the two-diode equation. The case of *I–V* curves with both high and low sampling frequencies is addressed. We assess the robustness of our fit procedure on a wide population of solar cells featuring different electrical parameters. We then broaden our method to the cases of J_{sc} and V_{oc} extraction from the *I–V* curves. We then show the validity of our approach by extracting P_{max} from *I–V* curves measured on actual devices.

II. EXPERIMENTAL DETAILS

A. Generation of Synthetic I–V Curves

We generate *I–V* curves by numerically solving the two-diode equation (1) in steady state using the commercially available software MATLAB [23]

$$J = J_L - J_{01}\left\{\exp\left[\frac{q\,(V + JR_s)}{n_1 kT}\right] - 1\right\} - J_{02}\left\{\exp\left[\frac{q\,(V + JR_s)}{n_2 kT}\right] - 1\right\} - \frac{V + JR_s}{R_p}. \quad (1)$$

The inputs to (1) are Boltzmann's constant (k), the device temperature (T), the light-generated current density (J_L), the first and second diode saturation current densities (J_{01} and J_{02}, respectively), associated ideality factors (n_1 and n_2, respectively), and the shunt (R_p) and series (R_s) resistances (given in $\Omega{\cdot}cm^2$). In all the following, T is fixed to 298 K, n_1 = 1, and n_2 = 2. We also specify the position and the density of the voltage points (V), for which the two-diode equation (1) is solved, as further explained in the next paragraph below. The outputs of our model are the *I–V* and power–voltage (*P–V*) curves for a given set of $(J_L, J_{01}, n_1, J_{02}, n_2, R_s, R_p)$ values, as well as the calculated (theoretical) values for J_{sc}, V_{oc}, fill factor (FF), and P_{max} corresponding to this parameters set. These values are named $J_{sc,th}, V_{oc,th}$, FF_{th}, and $P_{max,th}$, respectively. At this stage, the determination of $J_{sc,th}, V_{oc,th}$, FF_{th}, and $P_{max,th}$ is only limited by the numerical accuracy of the solving algorithms of MATLAB, which is typically well below 10^{-5}% [24].

TABLE II
VALUES OF $(J_L, J_{01}, J_{02}, R_s, R_p)$ USED AS INPUT PARAMETERS TO OUR MODEL

J_L [mA/cm^2]	J_{01} [A/cm^2]	J_{02} [A/cm^2]	$R_s\,[\Omega \cdot cm^2]$	$R_p\,[\Omega \cdot cm^2]$
36.5–39.5	10^{-14}–10^{-12}	10^{-9}–10^{-7}	0.3–1.8	10^2–10^5

The output *I–V* curves of our model are called synthetic curves to differentiate them from the *I–V* curves experimentally measured on actual PV devices (see Section II-C). We distinguish two types of synthetic *I–V curves*: high-density curves (HD curves) and LD curves. HD curves are obtained when the two-diode equation (1) is solved for a high number of equally spaced voltage points. These curves correspond to the case where a high sampling frequency is used during the actual *I–V* measurement. In this paper, we chose 1 mV^{-1} as the sampling frequency for the synthetic HD curves. In contrast, LD curves are obtained when only sparse purposely placed voltage points are chosen, for instance, only a dozen of points placed at specific voltages along the full *I–V* curve. These LD curves are, thus, similar to the *DragonBack* approach proposed in [17] and [18]. The actual number and position of the voltage points we chose for the LD curves are further detailed in the Appendix.

In both cases, white Gaussian noise is added to the *I–V* and *P–V* curves, both on the current and the voltage channels, in order to simulate the effect of an actual measurement. The signal-to-noise ratio equals 80 dB for the current and the voltage channels.

Fig. 1 illustrates the overall principle of our model, from the input parameters to the output synthetic HD and LD *I–V* and *P–V* curves.

Using this model, we generate a virtual population of 500 solar cells (both for the HD and the LD curves cases) whose values for $(J_L, J_{01}, J_{02}, R_s, R_p)$ are randomly chosen into ranges containing representative values of these parameters for crystalline silicon-based PV cells [25]–[28]. The ranges used for $(J_L, J_{01}, J_{02}, R_s, R_p)$ are given in Table II. The resulting distributions of $J_{sc,th}, V_{oc,th}$, FF_{th}, and $P_{max,th}$ for the 500 solar cells are plotted in Fig. 2. This approach aims to generate *I–V* curves that feature a wide variety of shapes and key data, as could be actually encountered by research labs or customers

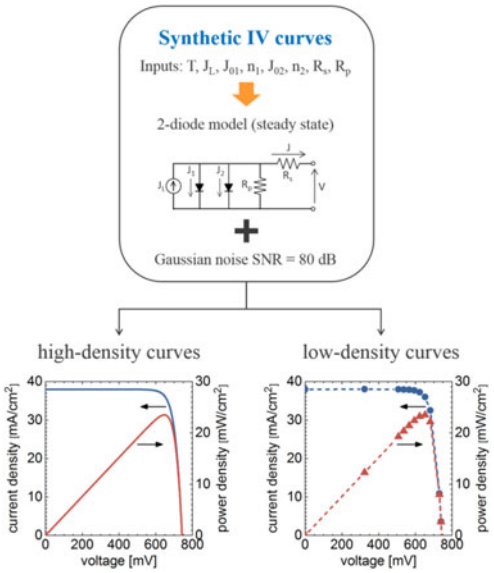

Fig. 1. Generation of synthetic *I–V* curves by numerically solving the two-diode equation in steady state. Two types of curves are produced: HD curves are obtained when the two-diode equation is solved for a high-voltage sampling frequency; LD curves are obtained when only sparse voltage points are used.

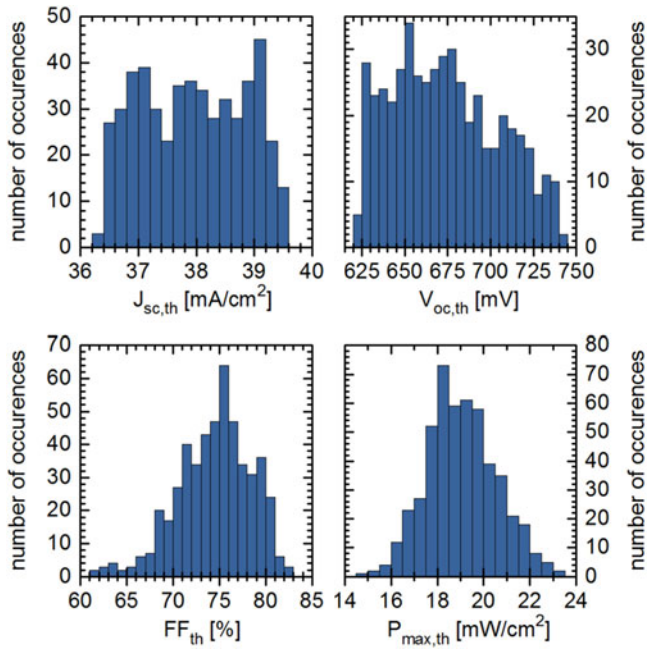

Fig. 2. Distribution of the theoretical values for J_{sc}, V_{oc}, FF, and P_{max} for the 500 solar cells population generated using the model presented in Fig. 1 and the input parameters of Table II.

measuring various solar cells technologies. We then test the robustness of the fitting procedures on this broad population, as detailed in Section III.

B. Fitting Procedures

For each solar cell within the population of Fig. 2, various fit procedures are performed in order to extract the value of P_{max} from the *P–V* curves. This experimentally fitted value is named $P_{max,fit}$ in the following. As presented in the bottom row

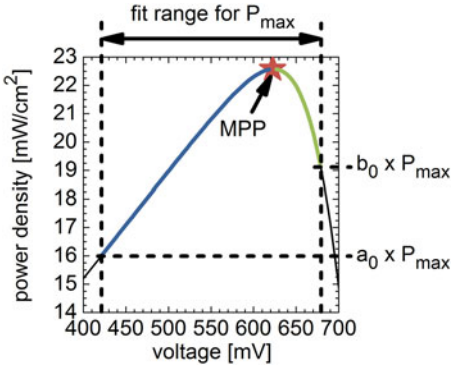

Fig. 3. Schematic of the fit range we consider in this paper to extract the solar cell peak power from its *P–V* curve. We use a polynomial regression of at least the fourth order. The fit range is defined as the (*P*, *V*) points such as $P \geq a_0 \times P_{max}$ for $V < V_{mpp}$ and $P \geq b_0 \times P_{max}$ for $V \geq V_{mpp}$, where $0 < a_0 < 1$, and $0 < b_0 < 1$.

of Table I, we use a fourth-order polynomial fit. The (*P*, *V*) points on which the polynomial regression is performed are defined as $P \geq a_0 \times P_{max}$ for $V < V_{mpp}$, and $P \geq b_0 \times P_{max}$ for $V \geq V_{mpp}$. The parameters a_0 and b_0 can vary independently within 0 and 1. Importantly, note that in contrast with NREL [1], we define two independent thresholds, as a_0 is the threshold for voltages below V_{mpp}, whereas b_0 is the threshold for voltages above V_{mpp}. The resulting fit range for P_{max} is exemplarily illustrated in Fig. 3.

The fitted values are then compared with the theoretical ones, and the error on P_{max} is calculated for each single device as

$$\varepsilon\ (P_{max}) = \frac{P_{max,fit} - P_{max,th}}{P_{max,th}}\ . \tag{2}$$

According to (2), $\varepsilon(P_{max}) > 0$ indicates that the fitted value of P_{max} is an overestimation of the actual P_{max}. Conversely, $\varepsilon(P_{max}) < 0$ indicates an underestimation of the actual P_{max}. As benchmarks, we calculate $\varepsilon(P_{max})$ following the methods proposed by the ASTM standard [22] and NREL [1], as reported in Table I, for the same solar cell population.

From an economical point of view, an underestimation or an overestimation of P_{max} are equally detrimental. Moreover, an efficient fit procedure should result robust on devices featuring very different key data. Hence, the absolute value of $\varepsilon(P_{max})$ is computed and averaged on the 500 solar cells under investigation. This value is hereafter referred to as $\overline{|\varepsilon(P_{max})|}$. When required, the two-sigma standard deviation (2σ) values of $\overline{|\varepsilon(P_{max})|}$ is also calculated. We, thus, report the overall error $\tilde{\varepsilon}(P_{max})$ as

$$\tilde{\varepsilon}\ (P_{max}) = \overline{|\varepsilon\,(P_{max})|}\ \pm 2\sigma\,(|\varepsilon\,(P_{max})|)\,. \tag{3}$$

C. Measurement of Actual I–V Curves

We experimentally measured three solar cell technologies: passivated emitter and rear cell (PERC), interdigitated back-contact (IBC), and amorphous/crystalline silicon heterojunction (SHJ). Further details regarding the PERC, the IBC, and the SHJ technologies can be found in [29]–[31], respectively, and the references therein. For each technology, we measured both

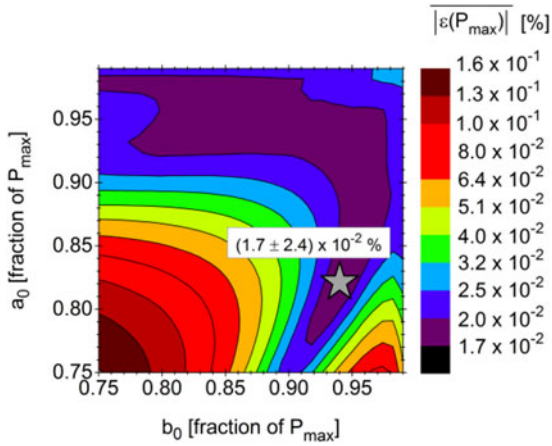

Fig. 4. Variation of the absolute value of the error on $P_{\max}$, averaged on 500 solar cells ($\overline{|\varepsilon(P_{\max})|}$), as a function of the (a_0, b_0) boundaries used for the fit range in the case of a fourth-order polynomial fit. The gray star indicates the position of the minimum for $\overline{|\varepsilon(P_{\max})|}$.

TABLE III
TECHNOLOGIES AND MEASURED KEY DATA OF THE SINGLE SOLAR CELLS INVESTIGATED IN THIS PAPER

Solar cell	J_{sc} [mA/ cm^2]	V_{oc} [mV]	FF [%]	Eff. [%]
IBC	40.5	709	78.3	22.5
PERC	40.0	663	79.3	21.0
SHJ	39.2	733	78.2	22.5

TABLE IV
TECHNOLOGIES AND MEASURED KEY DATA OF THE SOLAR MODULES INVESTIGATED IN THIS PAPER

Module	I_{sc} [A]	V_{oc} [V]	FF [%]	P_{max} [W]
IBC	6.19	69.04	79.2	337.9
PERC	9.43	39.26	74.9	277.2
SHJ	9.14	43.91	74.7	299.8

single solar cells and commercially available modules. The single solar cells were measured using a Wacom WXS-90S-L2 steady-state solar simulator in standard test conditions at 25 °C under AM1.5G equivalent illumination. The modules were measured on a Pasan High$^{\text{LIGHT}}$ 3 tunnel flasher. Table III (respectively, Table IV) summarizes the key data of the investigated single solar cells (respectively, modules), as obtained from the experimental *I–V* curves using our fit procedures. Remarkably, all three technologies reach conversion efficiencies >21.0% at cell level. Note, however, that for these experimentally measured *I–V* curves, the theoretical values of the key data remain unknown, in contrast with the case of the synthetic *I–V* curves, for which the theoretical values of the key data are known *a priori* (see Section II-A).

III. RESULTS AND DISCUSSION

A. Extraction of the Devices Peak Power From High-Density Synthetic I–V Curves

Fig. 4 reports the variation of $\overline{|\varepsilon(P_{\max})|}$ as a function of the values chosen for the (a_0,b_0) boundaries in the case of a fourth-order polynomial fit. The smaller the a_0 and b_0—i.e., the larger the fit range—the higher the $\overline{|\varepsilon(P_{\max})|}$. The minimum for $\overline{|\varepsilon(P_{\max})|}$ occurs at $a_0 = 0.82$ and $b_0 = 0.94$. For these boundaries, $\tilde{\varepsilon}\ (P_{\max}) = (2 \pm 2)\ \times 10^{-2}\%$. This error results notably lower than the ones obtained on the same solar cells population when applying the fit criteria of ASTM and NREL, as illustrated in Fig. 5. Indeed, the ASTM method yields $\tilde{\varepsilon}\ (P_{\max}) = (8 \pm 1)\ \times 10^{-2}\%$, and NREL $\tilde{\varepsilon}\ (P_{\max}) = (6 \pm 10)\ \times 10^{-2}\%$.

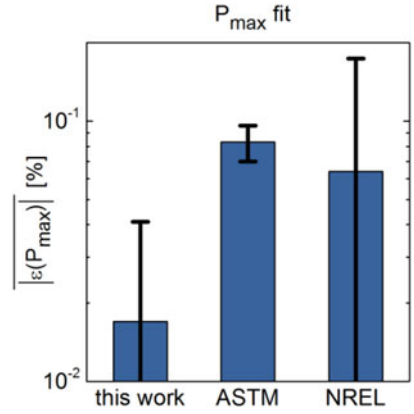

Fig. 5. Comparison of the absolute value of the error on $P_{\max}$, averaged on 500 solar cells ($\overline{|\varepsilon(P_{\max})|}$), for the method investigated in this publication, and the criteria suggested by ASTM [22] and NREL [1]. The error bars are the 2σ deviation of $|\varepsilon(P_{\max})|$ for the 500 solar cells under investigation.

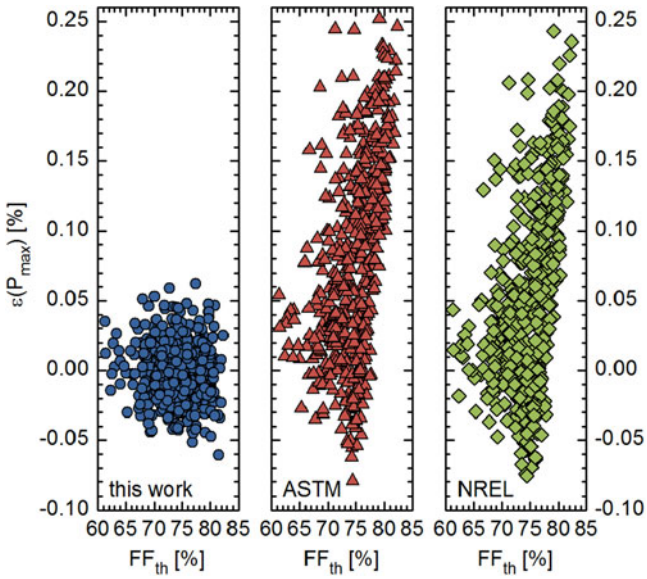

Fig. 6. Variation of the error on $P_{\max}$ as a function of the FF of the solar cells. Each data point represents one individual device from the 500 solar cells population under study (see Fig. 2).

Fig. 6 plots the values of $\varepsilon(P_{\max})$ as a function of $\mathrm{FF_{th}}$ of each individual solar cell among the population under study. For the ASTM and the NREL procedures, there is a clear correlation between $\varepsilon(P_{\max})$ and $\mathrm{FF_{th}}$: the higher the $\mathrm{FF_{th}}$, the larger the $\varepsilon(P_{\max})$. Interestingly, the ASTM and the NREL fits mainly result in overestimated $P_{\max}$ values, $\varepsilon(P_{\max})$ being positive.

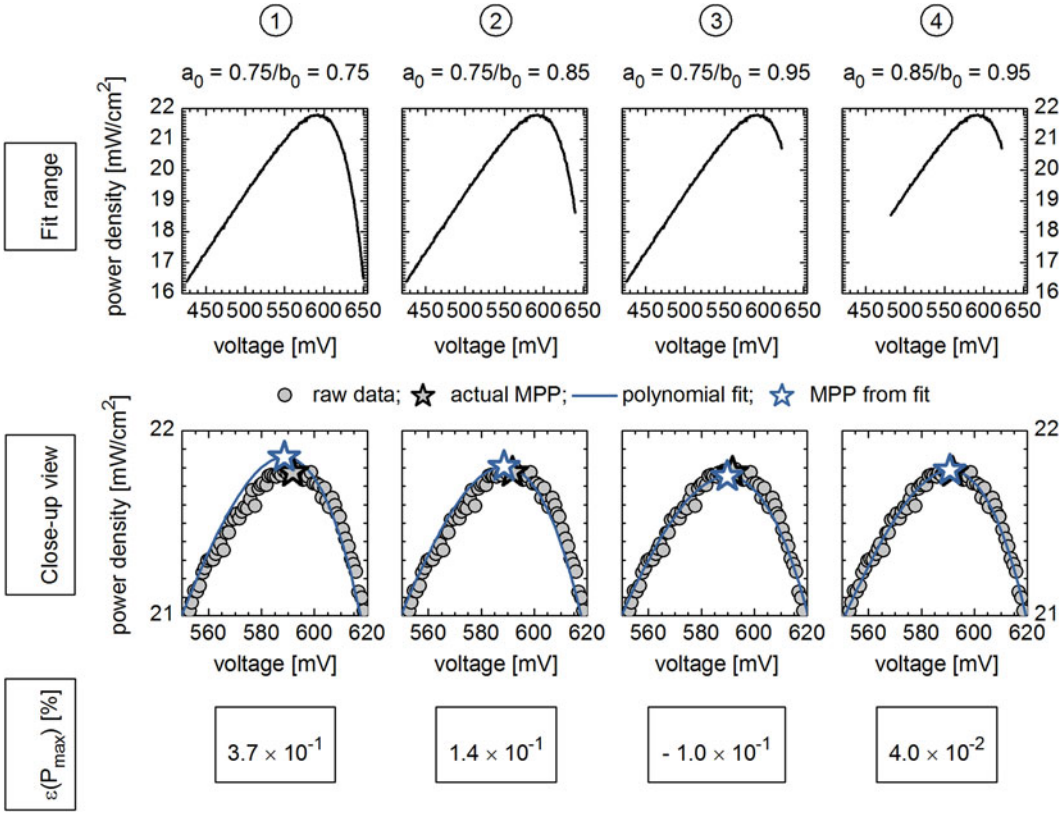

Fig. 7. $P_{\max}$ fit for a solar cell with FF = 82.3% (fourth-order polynomial fit) for different values of the a_0 and b_0 fit boundaries. The top row shows the range used for $P_{\max}$ fit, the middle row is a closeup view close to the MPP, and the bottom row gives the error between the fitted and the actual value of the MPP [$\varepsilon(P_{\max})$]. If symmetric boundaries are used (column ①), $P_{\max}$ is clearly overestimated. This error is sequentially reduced when using higher values for the right boundary b_0 (compare columns ② and ③ with ①) and, finally, adjusting the left boundary a_0 to higher value (column ④).

In contrast, our fit procedure does not show any correlation between $\mathrm{FF_{th}}$ and $\varepsilon(P_{\max})$. Moreover, the error on $P_{\max}$ is smaller with our fit ($|\varepsilon(P_{\max})| < 0.05\%$) than with the ASTM or the NREL ones ($|\varepsilon(P_{\max})| < 0.25\%$).

We affirm that this trend owes to the asymmetric shape of the *P–V* curve: Indeed, the *P–V* curve is usually steeper for voltages over V_{mpp} than for voltages below. As a result, if too many data points from the steep part of the *P–V* curve are included into the fit region, the polynomial fit has to feature a strong curvature at its maximum to accommodate for the steep slope. This results in an overestimation of $P_{\max}$ for devices with high FF, which usually exhibit very steep slope above V_{mpp}. This overestimation is a typical feature of the ASTM and the NREL fits, in which symmetrical boundaries are used for the $P_{\max}$ fit (see Table I). In contrast, our fit procedure enables to independently set the fit boundaries for voltages below and above V_{mpp}, thus alleviating this phenomenon. This point is illustrated in Figs. 7 and 8. We chose the solar cell featuring the highest $\mathrm{FF_{th}}$ among the population under study, namely 82.3%. For this solar cell, if $P_{\max}$ is extracted using the same value for the left and the right boundary (e.g., $a_0 = b_0 = 0.75$, see Fig. 7, column ①), then $P_{\max}$ is clearly overestimated, and $\varepsilon(P_{\max}) = 3.7 \times 10^{-1}\%$. In contrast, this error is sequentially reduced if higher values are used for the right boundary $\mathrm{b_0}$: compare columns ② and ③ with ①. Finally, adjusting the left boundary a_0 to a higher value further reduces the error (see column ④ in Fig. 7).

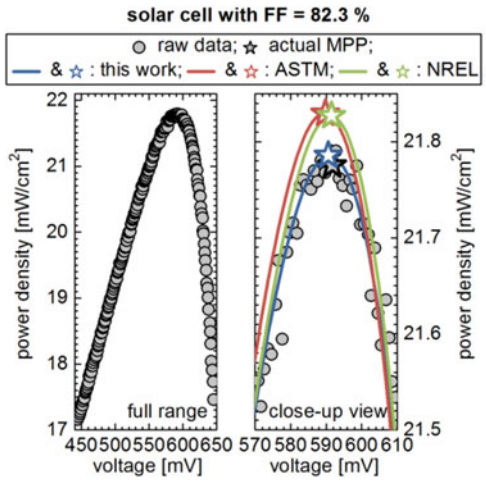

Fig. 8. (Left) Full range of raw data. (Right) Closeup view of the MPP region showing a comparison of the polynomial fits (solid lines) and the MPPs (stars) obtained using the $P_{\max}$ fit criteria proposed in this contribution, compared with those given by ASTM [22] and NREL [1].

Fig. 8 reports the polynomial fits and the MPPs obtained with our fit procedure, ASTM, and NREL and compares them to the

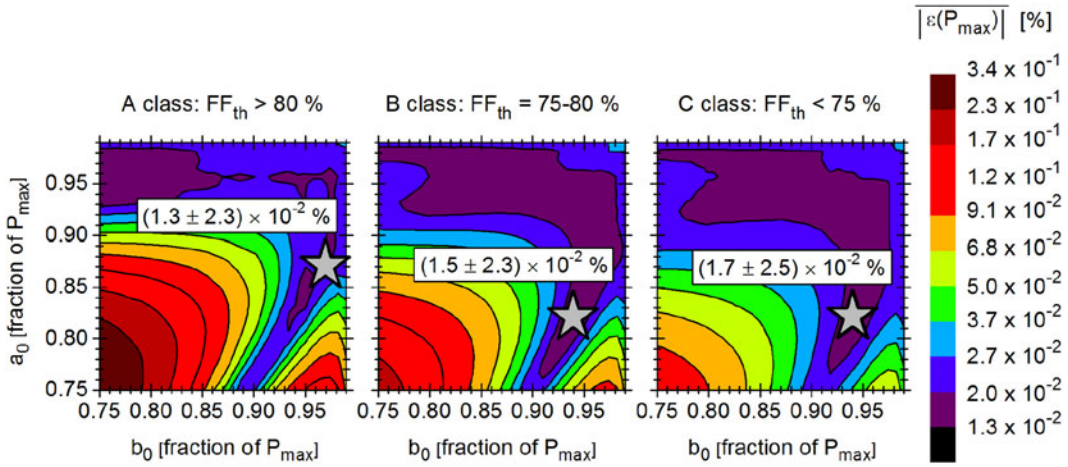

Fig. 9. Influence of the fit boundaries (a_0, b_0) on the absolute value of the error on $P_{\max}$, averaged on 500 solar cells ($\overline{|\varepsilon(P_{\max})|}$), and performed for different FF classes. The gray stars indicate the position of the minimum for $\overline{|\varepsilon(P_{\max})|}$.

actual MPP. For the reasons explained above, the ASTM and the NREL fits result in a clear overestimation of $P_{\max}$, whereas our approach yields a more accurate value.

This result suggests that the fit boundaries have to be adjusted as a function of the solar cell FF, in order to yield the highest possible accuracy. To investigate this possibility, we divided the solar cells population under test into three classes, according to their $\mathrm{FF_{th}}$: A class is for solar cells with $\mathrm{FF_{th}} \geq 80\%$, B class for $75\% \leq \mathrm{FF_{th}} < 80\%$, and C class for $\mathrm{FF_{th}} < 75\%$. For each of these classes, we carried out the (a_0,b_0) mapping, as done in Fig. 4. The results are plotted in Fig. 9. For B and C classes, the minimum value of $\overline{|\varepsilon(P_{\max})|}$ is obtained for the same boundaries, as in Fig. 4, namely $a_0 = 0.82$ and $b_0 = 0.94$, and equals $\approx 2 \times 10^{-2}\%$ for both classes. Importantly, the extraction of $P_{\max}$ for the solar cells from B and C classes results weakly sensitive to the fit boundaries: Indeed, $\overline{|\varepsilon(P_{\max})|}$ remains below 0.15%, regardless of the (a_0, b_0) values. In contrast, for A class solar cells, $\overline{|\varepsilon(P_{\max})|}$ is strongly sensitive to the fit boundaries: Especially, $\overline{|\varepsilon(P_{\max})|}$ goes up to 0.3% for small a_0 and b_0 values, e.g., 0.75, which corresponds to a large fit range for $P_{\max}$. Conversely, class A solar cells can be fitted more accurately if a narrower fit range is used, namely $a_0 = 0.87$ and $b_0 = 0.97$. For this range, $\tilde{\varepsilon}(P_{\max})$ drops down to $(1 \pm 2) \times 10^{-2}\%$, which is actually slightly lower than what can be achieved for solar cells from B and C classes.

We now turn to the effects of the choice of the polynomial order. Fig. 10 plots $\overline{|\varepsilon(P_{\max})|}$ as a function of the polynomial order. When a fourth-order polynomial is used, our fit procedure yields a notably better accuracy than the ASTM and the NREL fits, as already reported in Fig. 5. Using a fifth-order polynomial strongly reduces the error for the ASTM and the NREL fits, whereas our procedure is only marginally improved. When a sixth-order polynomial is used, the three fit methods yield similar accuracies. No further improvements are obtained with even higher order polynomials (not shown). This accuracy improvement with up to sixth-order polynomials is consistent with what Emery and Osterwald observed for a GaInP/GaAs solar cell [19]. However, great care must be given when handling high-order polynomial fits, as parasitic oscillations—known as Runge's phenomenon—can appear [32].

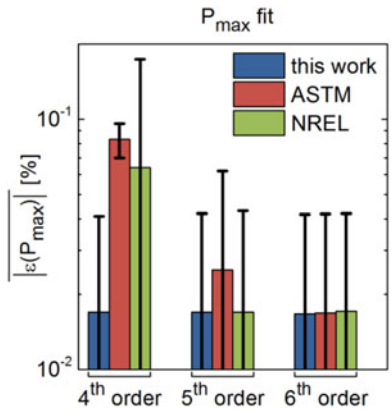

Fig. 10. Comparison of the absolute value of the error on $P_{\max}$, averaged on 500 solar cells ($\overline{|\varepsilon(P_{\max})|}$), for the method investigated in this publication and the criteria suggested by ASTM [22] and NREL [1] as a function of the polynomial order. The error bars are the 2σ deviation of $|\varepsilon(P_{\max})|$ for the 500 solar cells under investigation.

B. Extraction of the Devices Peak Power From Low-Density Synthetic I–V Curves

Based on the outcomes of Section III-A, we hypothesized that the optimum fit range determined for the HD curves—namely $a_0 = 0.82$ and $b_0 = 0.94$—will also apply to the LD curves. Within these boundaries, the unknown parameters that remain to be determined for the LD curves are 1) the number of data points to be placed around $\mathrm{P_{max}}$ and 2) their exact position.

Fig. 11 plots the variation of $\overline{|\varepsilon(P_{\max})|}$ as a function of the number of points placed near $P_{\max}$ for our LD curves, in the case of a fourth-order polynomial fit. So far, these points are linearly spaced in voltage. With our procedure, the fit accuracy is only marginally improved when using more data points: for instance, five data points (i.e., the minimum number required for a fourth-order polynomial fit) already yields

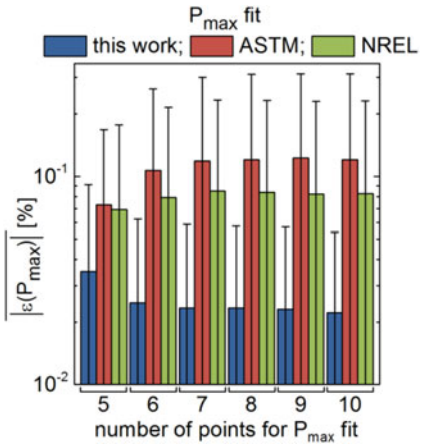

Fig. 11. Variation of the absolute value of the error on $P_{\max}$, averaged on 500 solar cells ($\overline{|\varepsilon(P_{\max})|}$), for the method investigated in this publication and the criteria suggested by ASTM [22] and NREL [1] as a function of the number of points placed near $P_{\max}$ for LD curves. The error bars are the 2σ deviation of $|\varepsilon(P_{\max})|$ for the 500 solar cells under investigation.

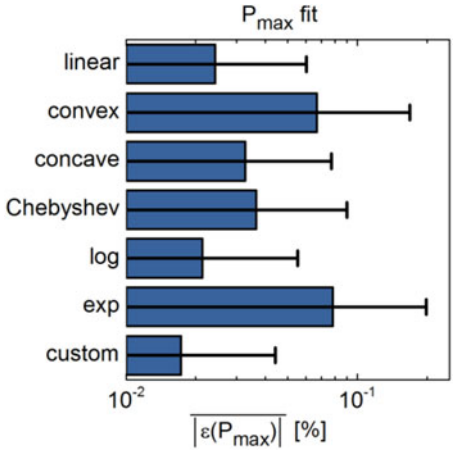

Fig. 12. Absolute value of the error on $P_{\max}$, averaged on 500 solar cells ($\overline{|\varepsilon(P_{\max})|}$), when using seven points with different spacings for $P_{\max}$ fit, as detailed in the Appendix. The error bars are the 2σ deviation of $|\varepsilon(P_{\max})|$ for the 500 solar cells under investigation.

$\tilde{\varepsilon}\,(P_{\max}) = (4 \pm 3)\ \times 10^{-2}\%$. With seven points, $\tilde{\varepsilon}\,(P_{\max}) = (2 \pm 2)\ \times 10^{-2}\%$, which is the same accuracy as reached on HD curves (see Section III-A). Adding additional points does not help to improve the accuracy in a great extent. If the ASTM or the NREL fits were used with only seven data points, the error would be $\tilde{\varepsilon}\,(P_{\max}) = (12 \pm 18)\ \times 10^{-2}\%$ and $\tilde{\varepsilon}\,(P_{\max}) = (8 \pm 15)\ \times 10^{-2}\%$, respectively.

Fig. 12 plots $\overline{|\varepsilon(P_{\max})|}$ in the case of seven data points with different spacings (cf., the Appendix for the definition of the spacing functions). Remarkably, the linear spacing performs already quite well. Only the logarithmic spacing and our custom function yield slightly better results. In contrast, the convex, concave, exponential spacing and the Chebyshev nodes result in larger errors. Indeed, with these spacings, the data points are clustered close to the first data point (convex spacing), the last one (concave, exponential spacing), or both outer points (Chebyshev nodes). As a consequence, the MPP region is poorly sampled and the polynomial fit result in an inaccurate extraction of $P_{\max}$.

TABLE V
FIT TYPES, FIT RANGES, AND ASSOCIATED TYPICAL ERRORS FOR THE EXTRACTION OF $J_{\rm sc}$, $V_{\rm oc}$, AND $P_{\rm MAX}$ IN THE CASE OF HD *I–V* CURVES

Parameter	Fit type	Fit range	Typical error* [%]
J_{sc}	Linear	$[-0.5; 0.5] \times V_{mpp}$	$(4 \pm 6) \times 10^{-3}$
V_{oc}	Linear	$[-0.1; 0.3] \times J_{mpp}$	$(5 \pm 7) \times 10^{-3}$
P_{max}	Fourth-order polynomial	$P \geq 0.82 \times P_{max}$ for $V < V_{mpp}$ $P \geq 0.94 \times P_{max}$ for $V \geq V_{mpp}$	$(2 \pm 2) \times 10^{-2}$

*The typical error is $\overline{|\varepsilon(X)|} \pm 2\sigma(|\varepsilon(X)|)$, where X = J_{sc}, V_{oc} or P_{max}.

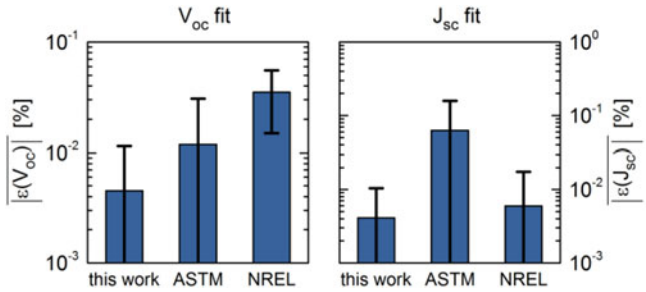

Fig. 13. Comparison of the absolute value of the error on $V_{\rm oc}$, averaged on 500 solar cells ($\overline{|\varepsilon(V_{\rm oc})|}$ on the left), and $J_{\rm sc}$ ($\overline{|\varepsilon(J_{\rm sc})|}$ on the right) for the method investigated in this publication and the criteria suggested by ASTM [22] and NREL [1] in the case of HD synthetic curves.

Overall, the improvement provided by the logarithmic or the custom spacing over the linear one is marginal. Moreover, the good accuracy of the custom spacing is mainly due to the fact that we calculated *a priori* the position of the MPP. Consequently, the generalization of such a custom function to any kind of solar cell appears questionable. Hence, we eventually assert that the linear spacing is the safest option regarding robustness.

Last but not least, the mapping of $P_{\max}$ as a function of the (a_0,b_0) boundaries in the case of seven linearly spaced points (best conditions according to Figs. 11 and 12) yields an optimum range close to $a_0 = 0.82$ and $b_0 = 0.94$ (data not shown). This thus validates the hypothesis we did at the beginning of this section.

C. Application to $J_{\rm sc}$ and $V_{\rm oc}$ Fits

Following the same approach as in Sections III-A and B, we also investigated the extraction of $J_{\rm sc}$ and $V_{\rm oc}$ from the *I–V* curves. The optimization of the fit ranges and methods was carried out similarly to what was done for $P_{\max}$ in the previous sections. Further details can be found in [33]. The best fit ranges and methods we identified are summarized in Table V. Fig. 13 plots the mean absolute error on $V_{\rm oc}$ and $J_{\rm sc}$, in the case of HD curves, and compared it with the values obtained following the guidelines of ASTM and NREL. For both $J_{\rm sc}$ and $V_{\rm oc}$, our fit parameters are more accurate than what could be obtained using the criteria of ASTM or NREL.

In the case of LD curves, we also carried out the optimization of the number of points and their position for the fit of $J_{\rm sc}$ and $V_{\rm oc}$, following the approach we proposed for $P_{\max}$ in

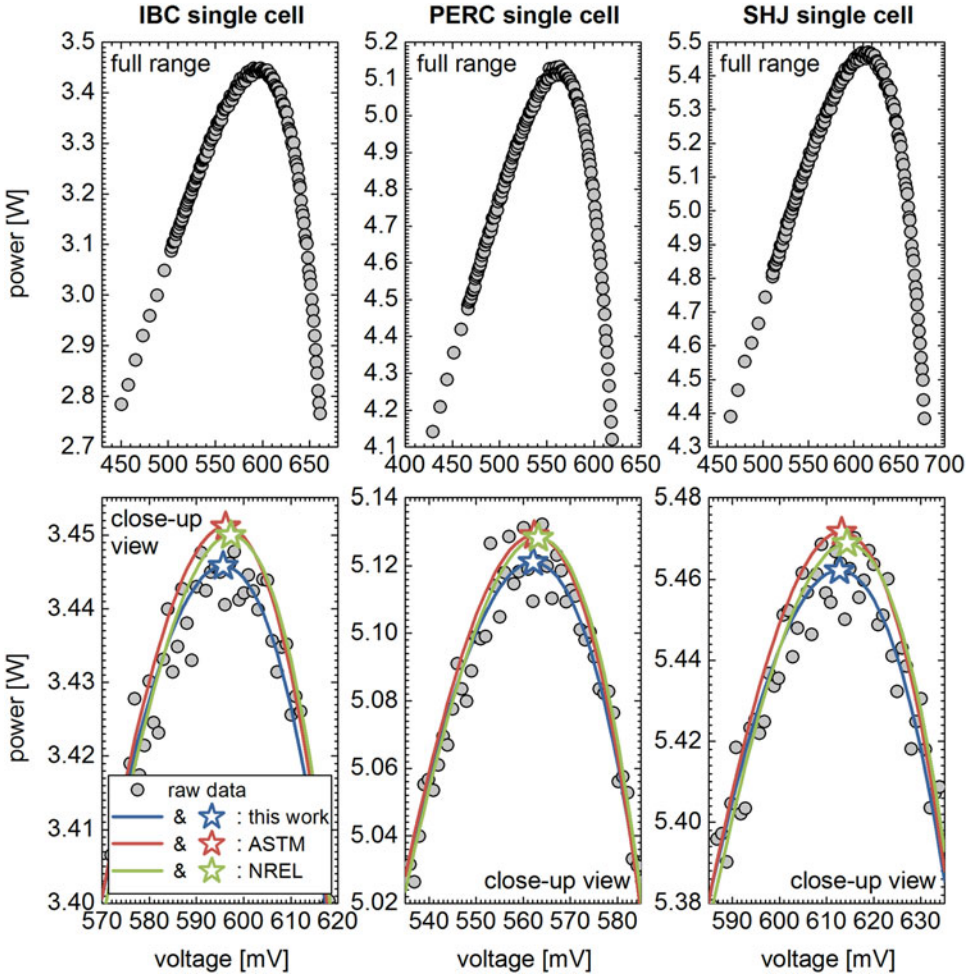

Fig. 14. (Top row) Full range of raw data. (Bottom row) Closeup view of the MPP region showing a comparison of the polynomial fits (solid lines) and the MPPs (stars) obtained using the $P_{\max}$ fit criteria proposed in this contribution, compared with those given by ASTM [22] and NREL [1], in the case of experimentally measured *P–V* curves of single solar cells.

TABLE VI
FIT TYPES, NUMBER OF DATA POINTS, FIT RANGES, AND ASSOCIATED TYPICAL ERRORS FOR THE EXTRACTION OF $J_{\rm sc}$,$V_{\rm oc}$, AND $P_{\rm MAX}$ IN THE CASE OF LD *I–V* CURVES

Parameter	Fit type (number of points)	Fit range	Typical error* [%]
$J_{\rm sc}$	Linear (two points)	$(-0.5, 0.5) \times V_{\rm mpp}$	$(2 \pm 4) \times 10^{-2}$
$V_{\rm oc}$	Linear (three points)	$(-0.1, 0.1, 0.3) \times J_{\rm mpp}$	$(4 \pm 2) \times 10^{-2}$
$P_{\max}$	Fourth-order polynomial (seven points)	$P \geq 0.82 \times P_{\max}$ for $V < V_{\rm mpp}$ $P \geq 0.94 \times P_{\max}$ for $V \geq V_{\rm mpp}$	$(2 \pm 2) \times 10^{-2}$

*The typical error is $\overline{|\varepsilon(X)|} \pm 2\sigma(|\varepsilon(X)|)$, where X $= {\rm J_{sc}}, {\rm V_{oc}}$ or $P_{\max}$.

Section III-B. As a result, we obtained $\tilde{\varepsilon}\,(J_{\rm sc}) = (2 \pm 4) \times 10^{-2}\%$ and $\tilde{\varepsilon}\,(V_{\rm oc}) = (4 \pm 2) \times 10^{-2}\%$. Note that only two points were used to fit $J_{\rm sc}$, and three points for $V_{\rm oc}$, as reported in Table VI.

D. Overview of the Fit Parameters

Tables V and VI provide an overview of the fit ranges and methods yielding the best accuracies for $J_{\rm sc}$, $V_{\rm oc}$, and $P_{\max}$, for the case of HD and LD curves, respectively.

Looking at Tables V and VI, it is to be noticed that the error on $J_{\rm sc}$ and $V_{\rm oc}$ is larger for the LD curves than for the HD ones: $\overline{|\varepsilon(J_{\rm sc})|}$ is indeed five times larger in the case of LD curves and $\overline{|\varepsilon(V_{\rm oc})|}$ eight times larger. This mainly owes to the fact that very few points were used for the fit of $J_{\rm sc}$ and $V_{\rm oc}$ in the LD curves: only two and three points, respectively. In contrast, $\overline{|\varepsilon(P_{\max})|}$ remains remarkably constant regardless of the curve type (HD or LD). This important result points out that $P_{\max}$ can actually be extracted with a very small number of points along the *I–V* curve, provided that these points are placed at the appropriate positions, as investigated in Section III-B.

Interestingly, the errors obtained using the guidelines we presented in this work are notably lower than those reported by Dirnberger and Kraling [3] for the fit procedures used at Fraunhofer ISE CalLab, these latter being namely $2.3 \times 10^{-2}\%$ for $J_{\rm sc}$, $3.8 \times 10^{-2}\%$ for $V_{\rm oc}$, and $4.4 \times 10^{-2}\%$ for $P_{\max}$.

E. Validation on Actual Photovoltaic Devices

Fig. 14 plots the *P–V* curves measured on single solar cells. For each solar cell technology, the ASTM and the NREL fits evidently overestimate $P_{\max}$, as expected from our numerical

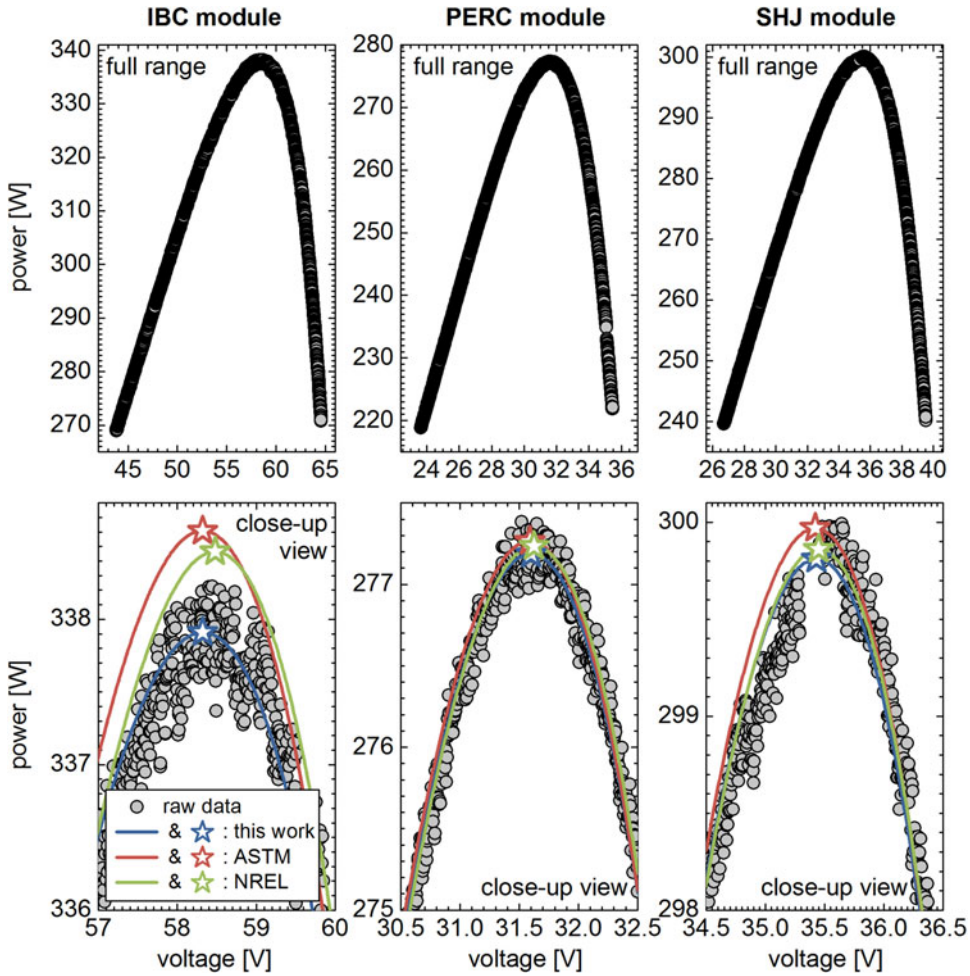

Fig. 15. (Top row) Full range of raw data. (Bottom row) Closeup view of the MPP region showing a comparison of the polynomial fits (solid lines) and the MPPs (stars) obtained using the $P_{\max}$ fit criteria proposed in this contribution, compared with those given by ASTM [22] and NREL [1], in the case of experimentally measured P–V curves of solar modules.

simulations. In contrast, the fit procedure developed in this paper yields a more realistic $P_{\max}$ value. For these three solar cells, the $P_{\max}$ values obtained following the ASTM and the NREL guidelines are typically $\sim$0.15% higher than those obtained using our fit criteria. This value is consistent with what was expected from our numerical simulations for single solar cells with FF of 78% to 79%.

Fig. 15 plots the P–V curves measured on PV modules. As for single solar cells, our fit gives a $P_{\max}$ value that is more in line with the experimental data. Remarkably, the overestimation of $P_{\max}$ made by the ASTM and the NREL fits scales with the module FF. Indeed, it is as high as 0.21% in the case of the IBC module—whose FF is 79.2%—whereas it shrinks down to $<$0.05% for the PERC and the SHJ modules, whose FF are $<$75%. This suggests that our fit guidelines, even if developed on numerical I–V curves of single solar cells, also apply when fitting full PV modules.

The LD curve (seven linearly spaced data points; see the bottom line of Table VI) of the PERC module is plotted in Fig. 16. As can be seen, the LD data points are perfectly in line with the HD curve. Moreover, the $P_{\max}$ value extracted using the seven LD points differs by only 3.3×10^{-2}% with the one based on the HD curve. Similar results are obtained for the IBC and the SHJ modules. This again validates our numerical simulations reported in Section III-B.

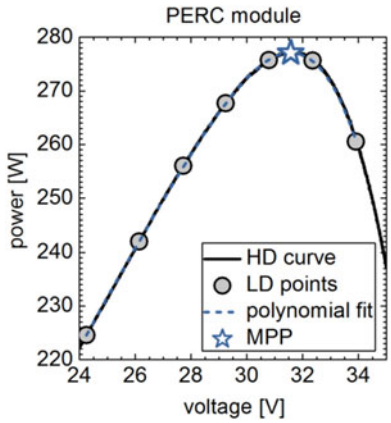

Fig. 16. LD points acquired on the PERC module under study in the case of seven linearly spaced data points. Note the perfect match with the HD curve. The MPP extracted with our fit procedure using the seven LD points differs by only 3.3×10^{-2}% with the one based on the HD curve.

F. Outlook

This paper evidenced that a thorough choice of the fit range and method is mandatory to accurately extract the key data of a solar cell or module from its *I–V* curve. Importantly, we found out that using two independent fit boundaries defined as a fraction of P_{max} yields a higher accuracy than with existing standards.

Although we affirm that our approach is of general validity, we would like to draw the reader's attention on the assumptions that were made throughout this paper. First of all, we remind that the *I–V* curves generated in the frame of this paper are obtained solving the two-diode equation in steady state. Even if this model is widely accepted for crystalline silicon-based PV cells and modules, numerous deviations to the ideal two-diode behavior have been reported. This is the case for crystalline silicon solar cells with a floating junction [34], as well as CIGS [35] and amorphous silicon [36] thin-film devices, to name a few. Therefore, the optimum fit boundaries to be applied might change depending on the specific features of the *I–V* curve under study. Moreover, we did not consider any transient effect affecting the shape of the *I–V* curve: Doing so requires solving the two-diode equation in the transient regime, as, for instance, proposed in [37]–[39]. As a result, the boundaries, the number of points, and the point positions given in this paper should be regarded as guidelines. In contrast, our global approach is of general validity and, hence, further applies to other PV technologies.

Last but not least, we mainly focused in this paper on the *I–V* curves of single solar cells. Therefore, the application of our method to PV modules is questionable. However, as presented in Section III-E above, the first experimental results indicate that our fit guidelines also apply to modules.

Doubtlessly however, the accurate modeling of the *I–V* curve of an actual PV module is much more complicated than the simple approach we followed here. Especially, the operating conditions (irradiance, temperature) [40], bypass diodes [41], and shading effects [42], [43] can severely affect the shape of the PV module *I–V* characteristic. More detailed models for these topics can be found in [44] and [45].

IV. Conclusion

In this paper, the extraction of the key data of PV devices from their *I–V* characteristics has been discussed.

By numerically solving the two-diode equation in steady state, we generated synthetic *I–V* curves—representative of commercially available PV technologies to date—that serve as basis to unveil the relevant fit criteria required to accurately extract the device key data. First, we showed that the extraction of the device peak power is highly sensitive to the chosen power range where the fit is performed and to the order of the polynomial fit in a lesser extent. Second, we revealed that for a given fit range, the higher the device fill factor, the higher the error made on the estimation of the peak power. Along these lines, we proposed a specific fit range for the peak power extraction, bounded by two independent power thresholds asymmetrically distributed around the MPP. Our fit guidelines eventually yield a more accurate estimation of the peak power than what could be achieved with the international standards established so far, particularly for devices with fill factors above 80%. As most PV technologies will actually reach such values in the next years, we assert that it is worth revising the existing standards taking into account our results.

We have also demonstrated that an equally accurate extraction of the peak power is achievable with only five to ten data points distributed at specific positions around the MPP.

Finally, we have validated our approach by extracting the key data of actual PV cells and modules.

Appendix

In the case of LD curves, the number *N* of data points needed to extract P_{max} cannot be smaller than $n_{\mathrm{poly}}+1$, where n_{poly} is the order of the polynomial used to fit P_{max}. As reported in Table I, we recommend the use of a polynomial regression of at least the fourth order. Hence, in our case, the minimum number of points for the LD curves is 5. Conversely, the maximum number of points is bounded by the time required to obtain stable values for the voltage and the current readings for each point. Considering a 10-ms flash duration, and the PV devices with the highest capacitance to date, Virtuani *et al.* [17] reported that about 20 stable (*I*, *V*) points can be acquired along the full *I–V* curve. Allocating half of these points to the fit of P_{max} is a reasonable hypothesis. Hence, we chose the maximum number of points used for P_{max} fit to be equal to 10.

Regarding the position of these data points, let $V_{\mathrm{LD}}(\mathrm{i})$ be the voltage position of the *i*th data point, where $1\leq \mathrm{i} \leq \mathrm{N}$. The positions $V_{\mathrm{LD}}(1)$ and $V_{\mathrm{LD}}(\mathrm{N})$ are already fixed by the a_0 and b_0 thresholds chosen for the P_{max} fit range, as illustrated in Fig. 3. Hence, the general expression for $V_{\mathrm{LD}}(\mathrm{i})$ is given as

$$\begin{aligned} &\forall\, i \ \in\ [1,\ N] \\ &V_{\mathrm{LD}}\,(i) = V_{\mathrm{LD}}\,(1) + \alpha\,(i)\cdot\left[V_{\mathrm{LD}}\,(N) - V_{\mathrm{LD}}\,(1)\right]. \end{aligned} \tag{4}$$

In (4), α is the spacing function and determines how the voltage points between $V_{\mathrm{LD}}(1)$ and $V_{\mathrm{LD}}(\mathrm{N})$ are spaced. Therefore, α must fulfill the following properties:

P1) be a monotonically increasing function;

P2) take values between 0 and 1;

P3) be such that $\alpha(1) = 0$ and $\alpha(N) = 1$.

The most straightforward way is, hence, to choose a linear function for α: In this case, the voltage points are equally spaced. Using the Chebyshev nodes is also a well-known possibility [32]. However, numerous other functions fulfill properties P1–P3 mentioned above. Table VII details α functions we investigate in this paper.

Note than in (5), $n=1$ gives a linear spacing (see the closed square symbols in Fig. 17). Choosing $n>1$ gives a convex curve; in contrast, $n<1$ yields a concave curve (see the closed circle symbols and the closed triangle symbols in the top left of Fig. 17 respectively). Also note that in (8), β and γ are calculated to ensure that properties P1–P3 are fulfilled. For the case $N=7$, $\beta = 2.725$ and $\gamma = -1.720$. For the sake of illustration, all these different α functions are plotted for the case $N=7$ in Fig. 17.

TABLE VII
GENERAL FORMULAS OF THE SPACING FUNCTIONS USED IN THIS PAPER TO DETERMINE THE POSITION OF THE DATA POINTS IN THE CASE OF SYNTHETIC LD *I–V* CURVES

Spacing type	General expression	
Polynomial spacing	$\alpha_n\ (i) = \frac{i^n - 1}{N^n - 1}$ with $n \in \mathbb{R}^{+*}$	(5)
Chebyshev nodes	$\alpha(i) = \frac{1}{2} \times (1 - \cos(\frac{\pi(i-1)}{N-1}))$	(6)
Logarithmic spacing	$\alpha(i) = (\frac{\ln(i)}{\ln(N)})^{1/2}$	(7)
Exponential spacing	$\alpha(i) = \beta(1 - e^{-i}) + \gamma$	(8)

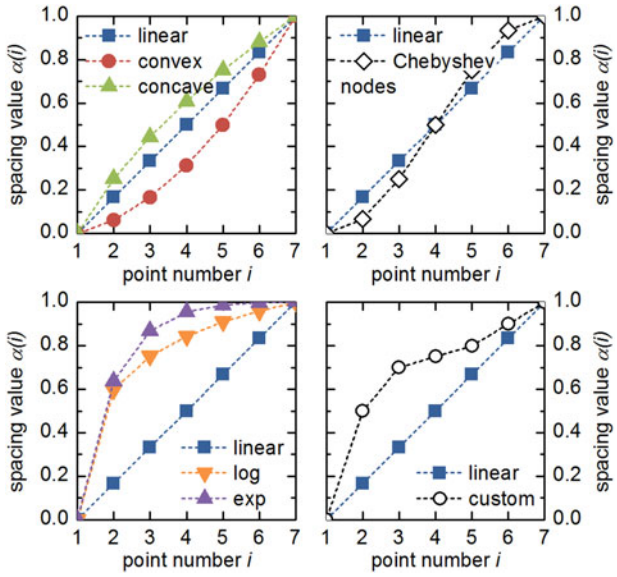

Fig. 17. Shapes of the spacing functions presented in Table VII when seven data points are placed in the fit range for P_{max} in the case of synthetic LD *I–V* curves.

Alternatively to (5)–(8), we also defined a "customized" expression for α by arbitrary choosing the value for each $\alpha(i)$, still fulfilling properties P1–P3. The aim of this custom function is to feature a higher point density close to the MPP. In the case of the 500 solar cells under study, the MPP is usually occurring at $\alpha \approx 0.75$. We, hence, purposely placed several points close to this value. The resulting custom function is plotted in the bottom right graph in Fig. 17.

REFERENCES

[1] K. Emery, "Measurement and characterization of solar cells and modules," in *Handbook of Photovoltaic Science and Engineering*, 2nd ed., A. Luque and S. Hegedus, Eds. New York, NY, USA: Wiley, 2011, pp. 701–752.

[2] "Guidelines for PV power measurement in industry," JRC Scientific and Technical Reports, compiled by partners in the Performance FP6 Integrated Project, 2010.

[3] D. Dirnberger and U. Kraling, "Uncertainty in PV module measurement—Part I: Calibration of crystalline and thin-film modules," *IEEE J. Photovoltaics*, vol. 3, no. 3, pp. 1016–1026, Jul. 2013.

[4] D. Dirnberger *et al.*, "Progress in photovoltaic module calibration: Results of a worldwide intercomparison between four reference laboratories," *Meas. Sci. Technol.*, vol. 25, Art. no. 105005, 2014.

[5] CTM-Group. International Technology Roadmap for Photovoltaic (ITRPV.net) Results 2014, Rev. 1, Jul. 2015.

[6] C. Monokroussos *et al.*, "Impact of calibration methodology into the power rating of c-Si PV modules under industrial conditions," in *Proc. 28th Eur. Photovoltaic Sol. Energy Conf.*, 2013, pp. 2926–2934.

[7] C. Monokroussos *et al.*, "Effects of spectrum on the power rating of amorphous silicon photovoltaic devices," *Prog. Photovoltaics, Res. Appl.*, vol. 19, pp. 640–648, 2011.

[8] V. Fakhfouri *et al.*, "Uncertainty assessment of PV power measurement in industrial environments," in *Proc. 26th Eur. Photovoltaic Sol. Energy Conf.*, 2011, pp. 3408–3412.

[9] S. Winter *et al.*, "Laser-DSR facility at PTB: Realization of a next generation high accuracy primary calibration facility," in *Proc. 27th Eur. Photovoltaic Sol. Energy Conf.*, 2012, pp. 3049–3051.

[10] M. C. López-Escalante, M. C. Fernandez, R. Sierras, and J. R. Ramos-Barrado, "Industrial solar cell tester: Study and improvement of I-V curves and analysis of the measurement uncertainty," *Prog. Photovoltaics, Res. Appl.*, vol. 24, pp. 108–121, 2016.

[11] G. Friesen and H. A. Ossenbrink, "Capacitance effects in high-efficiency cells," *Sol. Energy Mater. Sol. Cells*, vol. 48, pp. 77–83, 1997.

[12] J.-P. Kleider, J. Alvarez, A. Brézard-Oudot, M.-E. Gueunier-Farret, and O. Maslova, "Revisiting the theory and usage of junction capacitance: Application to high efficiency amorphous/crystalline silicon heterojunction solar cells," *Sol. Energy Mater. Sol. Cells*, vol. 135, pp. 8–16, 2015.

[13] P.-R. Beljean *et al.*, "I/V measurement of high capacitance cells with various methods," in *Proc. 26th Eur. Photovoltaic Sol. Energy Conf.*, 2011, pp. 3275–3278.

[14] H. Kojima, K. Iwamoto, A. Shimono, J. Abe, and Y. Hishikawa, "Accurate and rapid measurement of high-capacitance PV cells and modules using a single short pulse light," in *Proc. 40th IEEE Photovoltaic Spec. Conf.*, 2014, pp. 1896–1898.

[15] A. Virtuani *et al.*, "Results of the MPVT (Multi-Purpose PV Module Tester) project—A highly innovative and versatile solar simulator," in *Proc. 26th Eur. Photovoltaic Sol. Energy Conf.*, 2011, pp. 3424–3429.

[16] A. Virtuani and G. Rigamonti, "Performance testing of high-efficient highly-capacitive c-Si PV modules using slow-speed dark current-voltage characteristics and a reconstruction procedure," in *Proc. 28th Eur. Photovoltaic Sol. Energy Conf.*, 2013, pp. 2876–2881.

[17] A. Virtuani, G. Rigamonti, G. Friesen, D. Chianese, and P. Beljean, "Fast and accurate methods for the performance testing of highly-efficient c-Si photovoltaic modules using a 10 ms single-pulse solar simulator and customized voltage profiles," *Meas. Sci. Technol.*, vol. 23, Art. no. 115604, 2012.

[18] N. Ferretti, Y. Pelet, J. Berghold, V. Fakhfouri, and P. Grunow, "Performance testing of high-efficient PV modules using single 10 ms flash pulses," in *Proc. 28th Eur. Photovoltaic Sol. Energy Conf.*, 2013, pp. 3184–3187.

[19] K. A. Emery and C. R. Osterwald, "PV performance measurement algorithms, procedure and equipment," in *Proc. 21st IEEE Photovoltaic Spec. Conf.*, 1990, pp. 1068–1073.

[20] R. Gottschalg, M. Rommel, D. G. Infield, and M. J. Kearney, "The influence of the measurement environment on the accuracy of the extraction of the physical parameters of solar cells," *Meas. Sci. Technol.*, vol. 10, no. 9, pp. 796–804, Sep. 1999.

[21] H. Qasem *et al.*, "Analysis of key performance parameter extraction from current voltage measurements of photovoltaic devices," in *Proc. 37th IEEE Photovoltaic Spec. Conf.*, 2011, pp. 002283–002288.

[22] *Standard Test Method for Electrical Performance of Photovoltaic Cells Using Reference Cells Under Simulated Sunlight*, ASTM Int. Std. E948-09, 2009.

[23] *MATLAB Release 2012b*, The MathWorks, Inc., Natick, MA, USA, 2012.

[24] *fsolve Function*, The MathWorks, Inc., Natick, MA, USA, 2012.

[25] A. Khanna *et al.*, "A fill factor loss analysis method for silicon wafer solar cells," *IEEE J. Photovoltaics*, vol. 3, no. 4, pp. 1170–1177, Oct. 2013.

[26] T. F. Schulze, L. Korte, E. Conrad, M. Schmidt, and B. Rech, "Electrical transport mechanisms in a-Si:H/c-Si heterojunction solar cells," *J. Appl. Phys.*, vol. 107, pp. 1–13, 2010.

[27] B. Lim, T. Brendemühl, M. Berger, A. Christ, and T. Dullweber, "n-PERT back junction solar cells: An option for the next industrial technology generation?" in *Proc. 29th Eur. Photovoltaic Sol. Energy Conf.*, 2014, pp. 661–665.

[28] A. Fell *et al.*, "Input parameters for the simulation of silicon solar cells in 2014," *IEEE J. Photovoltaics*, vol. 5, no. 4, pp. 1250–1263, Jul. 2015.

[29] A. Quarteroni and F. Saleri, *Scientific Computing with MATLAB and Octave*, 2nd ed. New York, NY, USA: Springer, 2006.

[30] H. Hannebauer, T. Dullweber, U. Baumann, T. Falcon, and R. Brendel, "21.2%-efficient fineline-printed PERC solar cell with 5 busbar front grid," *Phys. Status Solidi—Rapid Res. Lett.*, vol. 8, no. 8, pp. 675–679, 2014.

[31] D. D. Smith *et al.*, "Toward the practical limits of silicon solar cells," *IEEE J. Photovoltaics*, vol. 4, no. 6, pp. 1465–1469, Nov. 2014.
[32] S. De Wolf, A. Descoeudres, Z. C. Holman, and C. Ballif, "High-efficiency silicon heterojunction solar cells: A review," *Green*, vol. 2, no. 1, pp. 7–24, Jan. 2012.
[33] B. Paviet-Salomon *et al.*, "New guidelines for a more accurate extraction of solar cells and modules key data from their current-voltage curves," *Prog. Photovoltaics, Res. Appl.*, 2016, submitted for publication.
[34] K. R. McIntosh, "Lumps, humps and bumps: Three detrimental effects in the current-voltage curve of silicon solar cells," Ph.D. dissertation, Centre Photovoltaic Eng., Univ. New South Wales, Sydney, Australia, 2001.
[35] M. Prorok, B. Werner, and T. Zdanowicz, "Applicability of equivalent diode models to modeling various thin-film photovoltaic (PV) modules in a wide range of temperature and irradiance conditions," *Electron. Technol.*, vols. 37/38, no. 3, pp. 1–4, 2005.
[36] J. Merten *et al.*, "Improved equivalent circuit and analytical model for amorphous silicon solar cells and modules," *IEEE Trans. Electron. Devices*, vol. 45, no. 2, pp. 423–429, Feb. 1998.
[37] C. Monokroussos *et al.*, "The effects of solar cell capacitance on calibration accuracy when using a flash simulator," in *Proc. IEEE 4th World Conf. Photovoltaic Energy Convers.*, 2006, pp. 2231–2234.
[38] B. Hu, B. Li, R. Zhao, and T. Yang, "Reflection-type single long-pulse solar simulator for high-efficiency crystalline silicon photovoltaic modules," *Rev. Sci. Instrum.*, vol. 82, p. 065104, 2011.
[39] M. Herman, M. Jankovec, and M. Topic, "Optimisation of the I-V measurement scan time through dynamic modelling of solar cells," *IET Renew. Power Gener.*, vol. 7, no. 1, pp. 63–70, 2013.
[40] V. Lo Brano, A. Orioli, G. Ciulla, and A. Di Gangi, "An improved five-parameter model for photovoltaic modules," *Sol. Energy Mater. Sol. Cells*, vol. 94, no. 8, pp. 1358–1370, 2010.
[41] S. Silvestre, A. Boronat, and A. Chouder, "Study of bypass diodes configuration on PV modules," *Appl. Energy*, vol. 86, no. 9, pp. 1632–1640, 2009.
[42] E. Karatepe, M. Boztepe, and M. Çolak, "Development of a suitable model for characterizing photovoltaic arrays with shaded solar cells," *Sol. Energy*, vol. 81, pp. 977–992, 2007.
[43] S. A. Spanoche, J. D. Stewart, S. L. Hawley, and I. E. Opris, "Model-based method for partially shaded PV module hot-spot suppression," *IEEE J. Photovoltaics*, vol. 3, no. 2, pp. 785–790, Apr. 2013.
[44] M. G. Villalva, J. R. Gazoli, and E. R. Filho, "Comprehensive approach to modeling and simulation of photovoltaic arrays," *IEEE Trans. Power Electron.*, vol. 24, no. 5, pp. 1198–1208, May 2009.
[45] F. Attivissimo *et al.*, "On the performance of the double-diode model in estimating the maximum power point for different photovoltaic technologies," *Meas. J. Int. Meas. Confederation*, vol. 46, no. 9, pp. 3549–3559, 2013.

Bertrand Paviet-Salomon was born in Lyon, France, in 1986. He received the M.Sc. degree and the Engineer Diploma degree in theoretical and applied optics, both in 2009, from the Institut d'Optique, Paris, France. From 2009 to 2012, he pursued the Ph.D. degree with the French National Institute for Solar Energy, Le-Bourget-du-Lac, France, working on laser processes for crystalline silicon solar cells. He received the Ph.D. degree in electronics and photonics from the University of Strasbourg, Strasbourg, France, in 2012.

From 2012 to 2014, he was a Postdoctoral Researcher with the Photovoltaics and Thin-Film Electronics Laboratory, École Polytechnique Fédérale de Lausanne, Neuchâtel, Switzerland, working on high-efficiency back-contacted silicon heterojunction solar cells. In 2014, he joined the PV-Center, Centre Suisse d'Électronique et de Microtechnique, Neuchâtel. His research interests include the development of high-efficiency crystalline silicon solar cells and modules.

Jacques Levrat received the Master of Physics degree with specialization in optics and semiconductor physics from the Swiss Federal Institute of Technology (EPFL), Lausanne, Switzerland, in 2008. In 2012, he received the Ph.D. degree from EPFL, where he was involved in the development of novel coherent light sources based on III-nitride microstructures.

His thesis on polaritonic nonlinear effects in GaN-based microcavities received an award from the Dimitris N. Chorafas foundation. In 2013, he joined the PV-Center, Centre Suisse d'Électronique et de Microtechnique, Neuchâtel, Switzerland, where he is in charge of simulations and metrological developments for c-Si solar cells and modules.

Vahid Fakhfouri, photograph and biography not available at the time of publication.

Yanik Pelet, photograph and biography not available at the time of publication.

Nicolas Rebeaud, photograph and biography not available at the time of publication.

Matthieu Despeisse received the Degree in electrical engineering from the Institut National des Sciences Appliquées de Lyon, Lyon, France, in 2002 and the Ph.D. degree from the European Organization for Particle Physics (CERN), Geneva, Switzerland, in 2006 for his work on amorphous silicon sensors deposited directly on the readout electronics.

He was with the CERN until 2008. His research focused on novel silicon radiation sensors (3-D, SiPM, a-Si:H), advanced microelectronics, and technology transfer. He then joined the Photovoltaics and Thin-Film Electronics Laboratory, École Polytechnique Fédérale de Lausanne, Neuchâtel, Switzerland, in 2009 to lead the research team working on thin-film silicon photovoltaics technology. Since 2013, he has been leading the research activities on crystalline silicon photovoltaics with the PV-center, Centre Suisse d'Électronique et de Microtechnique, Neuchâtel, with a special focus on silicon heterojunction technology, passivating contacts, and metallization.

Christophe Ballif received the Graduate degree in physics and the Ph.D. degree from the École Polytechnique Fédérale de Lausanne (EPFL), Lausanne, Switzerland, in 1994 and 1998, respectively, focusing on novel photovoltaic materials.

He was a Postdoctoral Researcher with the National Renewable Energy Laboratory, Golden, CO, USA. He then was with the Fraunhofer ISE, Freiburg, Germany, where he was involved in crystalline silicon photovoltaics (monocrystalline and multicrystalline) until 2003. He then joined the Swiss Federal Laboratories for Materials Science and Technology, Thun, Switzerland, before becoming a Full Professor and Chair with the Institute of Microengineering, University of Neuchâtel, Neuchâtel, Switzerland, in 2004. In 2009, the Institute was transferred to EPFL. He is the Director of the Photovoltaics and Thin-Film Electronics Laboratory within the Institute, as well as of the PV-Center, Centre Suisse d'Électronique et de Microtechnique, Neuchâtel, where he is dedicated to industrial research and technology transfer.